Topological superconductivity at finite temperatures in proximitized magnetic nanowires

Anna Gorczyca-Goraj,[1] Tadeusz Domański,[2] and Maciej M. Maśka[1,*]
[1]*Department of Theoretical Physics, University of Silesia, 40-007 Katowice, Poland*
[2]*Institute of Physics, M. Curie Skłodowska University, 20-031 Lublin, Poland*

(Received 27 February 2019; revised manuscript received 15 May 2019; published 26 June 2019)

Performing Monte Carlo simulations, we study the temperature-dependent self-organization of magnetic moments coupled to itinerant electrons in a finite-size one-dimensional nanostructure proximitized to a superconducting reservoir. At low temperatures, an effective interaction between the localized magnetic moments, that is mediated by itinerant electrons, leads to their helical ordering. This ordering, in turn, affects the itinerant electrons, inducing the topologically nontrivial superconducting phase that hosts the Majorana modes. In a wide range of system parameters, the spatial periodicity of a spiral order that minimizes the ground-state energy turns out to promote the topological phase. We determine the correlation length of such spiral order and study how it is reduced by thermal fluctuations. This reduction is accompanied by suppression of the topological gap (which separates the zero-energy mode from continuum), setting the upper (critical) temperature for the existence of the Majorana quasiparticles. Monte Carlo simulations do not rely on any ansatz for configurations of the localized moments, therefore, they can be performed for arbitrary model parameters, also beyond the perturbative regime.

DOI: 10.1103/PhysRevB.99.235430

I. INTRODUCTION

Recent progress in fabricating artificial nanostructures with spatial constraints [1] enabled observation of novel quantum states [2] where topology plays a prominent role. Motivated by the seminal paper of Kitaev [3], one of such intensively explored fields is related to topological superconductivity which occurs in semiconducting nanowires proximitized to superconductors [4–11] or nanochains of magnetic atoms deposited on superconducting surfaces [12–17]. In both cases, the Majorana-type quasiparticles have been observed at boundaries of proximitized nanoscopic wires/chains, and non-Abelian statistics [18] makes them promising for realization of quantum computing [19,20] and/or new spintronic devices [21].

A mechanism that drives the proximitized nanowire into a topologically nontrivial phase can originate from the spin-orbit coupling combined with the Zeeman splitting above some critical value of magnetic field [22–25]. Upon approaching this transition, a pair of finite-energy (Andreev) bound states coalesces into the degenerate Majorana quasiparticles [26,27] formed near the ends of the nanowire. Another scenario combines the proximity-induced superconducting state with the spiral magnetic order [28–48]. The latter approach is particularly appealing because magnetic order seems to adjust its periodicity (characterized by the pitch vector q_*) to support the topological phase. Origin of the topological phase in a system with spirally ordered magnetic moments is mathematically equivalent to the scenario based on the spin-orbit and Zeeman interactions [34,49]. Its *topofilia* (such terminology was introduced in Ref. [35] to emphasize that spatial profile of the spiral magnetic order self-tunes to external conditions in a way, guaranteeing the ground state of this system to be in a topological phase) has been investigated by a number of groups [32,42,47,48].

Topological features of the systems with self-organized spiral ordering have been, so far, studied, focusing mainly on the zero-temperature limit. Thermal effects have been partly addressed, taking into account magnon excitations (which suppress a magnitude of the spiral order) [34,42] and investigating a contribution of the entropy term to the free energy (which substantially affects the wave vector of the spiral order so that magnetic order might be preserved but the electronic state could no longer be topological) [47]. Usually, however, any long-range order hardly exists in one-dimensional (1D) systems at finite temperatures, and therefore, it is important—especially for practical applications of such systems—to estimate the maximum temperature up to which the topologically nontrivial states could survive. For its reliable determination, we perform here the Monte Carlo (MC) simulations.

Our numerical results unambiguously indicate that thermal effects are detrimental to both the topological superconducting state and the Majorana quasiparticles. This is evidenced by:

(i) changeover of the topological $\mathbb{Z}_2$ number,

(ii) characteristic scaling of the temperature-dependent coherence length of the spiral magnetic order,

(iii) and directly from the quasiparticle spectrum where thermal effects suppress the topological energy gap converting the zero-energy quasiparticles into overdamped modes.

The rest of the paper is organized as follows. In Sec. II, we introduce the microscopic model. Next, in Sec. III, we briefly revisit the topologically nontrivial superconducting state at zero temperature and check if it really coincides with the spiral pitch q_* that minimizes the ground-state energy. Essential results of our paper are presented in Sec. IV where we analyze (dis)ordering of the magnetic moments at finite

*maciej.maska@phys.us.edu.pl

temperatures by means of the MC method determining the upper (critical) temperature for the existence of the topological superconducting state and the Majorana quasiparticles. In Sec. V, we address the case beyond coplanar ordering. Finally, in Sec. VI, we summarize the main results.

II. MODEL

We consider a chain of the localized magnetic impurities whose moments are coupled to the spins of itinerant electrons. This nanoscopic chain is deposited on a surface of *s*-wave bulk superconductor, through the proximity effect inducing electron pairing. The setup is illustrated in Fig. 1. Such a system can be described by the following Hamiltonian:

$$H = -t\sum_{i,\sigma}\hat{c}^{\dagger}_{i,\sigma}\hat{c}_{i+1,\sigma} - \mu\sum_{i,\sigma}\hat{c}^{\dagger}_{i,\sigma}\hat{c}_{i,\sigma} + J\sum_{i}\boldsymbol{S}_i\cdot\hat{\boldsymbol{s}}_i + \sum_{i}(\Delta\hat{c}^{\dagger}_{i\uparrow}\hat{c}^{\dagger}_{i\downarrow} + \text{H.c.}), \tag{1}$$

where $\hat{c}^{\dagger}_{i,\sigma}$ and $\hat{c}_{i,\sigma}$ are the creation and annihilation operators of an electron at site i and $\hat{\boldsymbol{s}}_i$ is their spin,

$$\hat{\boldsymbol{s}}_i = \frac{1}{2}\sum_{\alpha,\beta}\hat{c}^{\dagger}_{i,\alpha}\boldsymbol{\sigma}_{\alpha\beta}\hat{c}_{i,\beta}, \tag{2}$$

with $\boldsymbol{\sigma}$ being a vector of the Pauli matrices. We assume that magnetic moments $\boldsymbol{S}_i$ have much slower dynamics than electrons and can be treated classically. In general, they can be expressed in the spherical coordinates in terms of the polar and azimuthal angles θ_i and ϕ_i,

$$\boldsymbol{S}_i = S(\sin\theta_i\cos\phi_i, \sin\theta_i\sin\phi_i, \cos\theta_i). \tag{3}$$

In the weak-coupling J limit, it has been shown [32,34,35] that the effective Ruderman-Kittel-Kasuya-Yosida (RKKY) interaction induces the helical ordering between the magnetic moments of the impurities,

$$\phi_i = iaq_*, \tag{4}$$

where a is the lattice constant and the spiral pitch q_* is strongly dependent on the model parameters [42,46]. Since Hamiltonian (1) has a SU(2) spin rotation symmetry for any constant opening angle θ_i without loss of generality, it can be assumed that $\theta_i = \pi/2$. It is possible to perform the gauge transformation, upon which the localized magnetic moments become ferromagnetically polarized at the expense of introducing the spin and q_*-dependent hopping amplitude [29]. Here, however, we are mostly interested in nonzero temperatures where the ground-state ordering is affected by thermal excitations. Therefore, we will treat ϕ_i's as fluctuating degrees of freedom. This will allow us not only to describe thermal states, but also to take into account possible phase separation where orderings with different values of q_* take place in segments of the nanochain [42,46]. We will also check the influence of θ_i fluctuations on the stability of the topological phase (Sec. V).

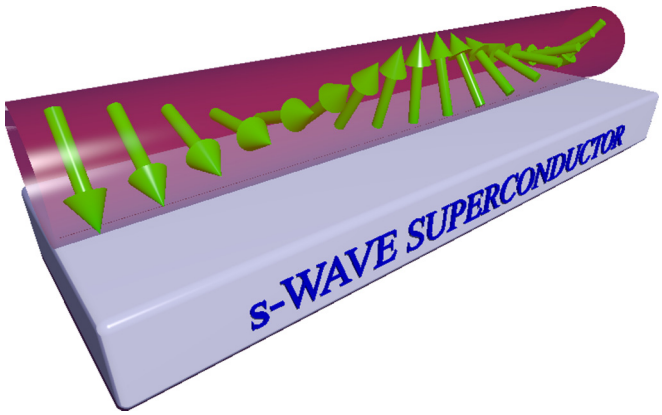

FIG. 1. A chain of magnetic impurities placed on top of a superconductor.

In what follows, we set the intersite spacing as a unit ($a = 1$) and impose $S = 1$ [50]. For simplicity we also set the Boltzmann constant $k_B \equiv 1$ and treat the hopping integral as a convenient unit ($t = 1$) for all energies discussed in our paper.

III. TOPOFILIA OF THE GROUND STATE

In the case of periodic boundary conditions, a spin-dependent gauge transformation can convert the Hamiltonian (1) into a translationally invariant form that can be easily diagonalized [29,35]. Here, however, we focus on the open boundary conditions that allows us to study the Majorana end states. Additionally, open boundary conditions do not impose any restrictions on the spiral pitch q, that is especially important for rather short nanochains. Most of our calculations have been performed for the nanowire comprising 70 sites. We have numerically diagonalized the system, considering various configurations of the local magnetic moments S_i. In particular, we have inspected the spiral ordering and considered $q \in [0;\pi]$ varying the model parameters J, μ, and Δ (transformation $q \to -q$ changes the chirality of the spiral, but it neither affects the thermodynamic nor the topological properties).

The ground state of the Hamiltonian (1) refers to some characteristic pitch $q = q_*$, which is determined from minimization of its energy. Since, in 1D metals, the static spin susceptibility diverges at $2k_F$, where k_F is the Fermi momentum, it has been suggested that also in the presence of the proximity-induced pairing the system will self-organize into a helical structure with the spiral pitch q_* coinciding with the momentum $2k_F$ [32,34,35]. However, even in the absence of the induced superconductivity, the spiral pitch that minimizes the ground-state energy can deviate from $2k_F$ if one goes beyond the Born approximation in the RKKY scheme [44]. We have investigated numerically the variation of the ground-state energy with respect to the model parameters and found that $q_* \approx 2k_F$, only in some regimes, whereas, generally, q_* can vary from 0 (fully polarized magnetic moments) to π/a (anitferromagnetic ordering). Figure 2(a) shows a typical example of the ground-state energy dependence on q.

To distinguish the trivial from nontrivial superconducting phases, we have computed the topological number $\mathbb{Z}_2$, determining it from the scattering matrix [51,52]. Here, we follow the procedure described in Ref. [28]. We have, thus, computed the scattering matrix S of the chain,

$$S = \begin{pmatrix} R & T' \\ T & R' \end{pmatrix}, \tag{5}$$

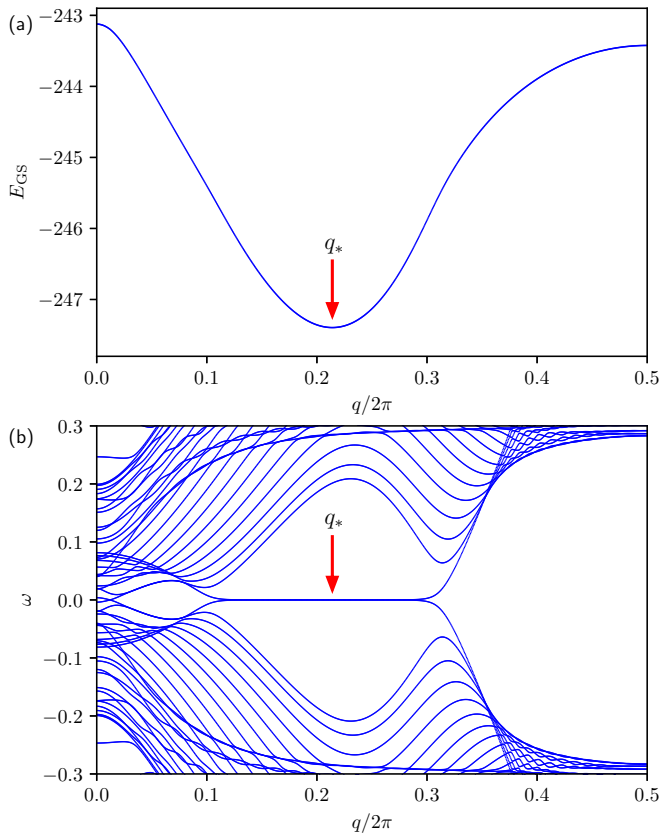

FIG. 2. (a) The ground-state energy E_{GS} versus the spiral pitch q obtained for $\Delta = 0.3$, $\mu = 1.5$, and $J = 1$. (b) Evolution of the quasiparticle spectrum with respect to q. The red arrows indicate q_*, minimizing the ground-state energy.

where R and T (R' and T') are 4×4 reflection and transmission matrices on the left (right) sides of the chain. This matrix (5) describes transport through the chain,

$$\begin{pmatrix} \psi_{-,\mathrm{L}} \\ \psi_{+,\mathrm{R}} \end{pmatrix} = S \begin{pmatrix} \psi_{+,\mathrm{L}} \\ \psi_{-,\mathrm{R}} \end{pmatrix}, \tag{6}$$

where $\psi_{\pm,\mathrm{L/R}}$ are the right- or left-moving modes ($\pm$) at the left or right edge (L/R) at the Fermi level. The topological quantum number is given by [28]

$$\mathcal{Q} = \mathrm{sgn}\,\det(R) = \mathrm{sgn}\,\det(R'). \tag{7}$$

The scattering matrix S can be obtained from multiplication of the individual transfer matrices of all the lattice sites. Since the product of numerous transfer matrices is numerically unstable, we converted them into a composition of the unitary matrices, involving only eigenvalues of the unit absolute value.

The spiral pitch q can, in general, be treated as an independent parameter, and we can study the topological properties of the Hamiltonian (1) as its function. Figure 3 shows $\det(R)$ versus q and Δ for $J = 2$ and several values of the chemical potential μ (analogous data have been obtained by us also for the stronger-coupling J). The topological phase corresponds to $\det(R) < 0$, and the nontopological phase corresponds to $\det(R) > 0$, respectively. In each panel, we display the spiral pitch q_* (yellow line) that minimizes the ground-state energy. Such curves resemble the results obtained previously in the weak-coupling limit J (see Fig. 3 of Ref. [53]). Let us remark that, for the wide range of model parameters, the spiral pitch $q_*(\Delta)$ indeed coincides with the topological region. It means that the system has a natural tendency towards self-adjusting the local magnetic moments in a way that guarantees the topologically nontrivial superconducting state [32,35,48]. Nevertheless, closer inspection of Fig. 3 reveals that such a tendency is not universal. For instance, for $\mu = 0.5$, the topological region does not overlap with q_*. Also, for $\mu = 2.5$, the topological state exists for $0.08 \lesssim \Delta \lesssim 0.87$, but it coincides with q_* only in a narrow regime $0.52 \lesssim \Delta \lesssim 0.72$. Figure 4 shows examples of the topological phase diagrams with respect to Δ and μ for the nanochain consisting of 70 sites, assuming the stable spiral orderings $q = q_*$. The role of the finite-size effects is presented in the Appendix (Fig. 19). We noted that with increasing length L the topological regions gradually expand and their boundaries become sharper.

IV. ROLE OF THERMAL EFFECTS

The influence of finite temperatures on the model (1) can be seen in a twofold way: By thermal broadening of the Fermi-Dirac distribution function of itinerant electrons and by a disturbance induced among the classical local moments $\boldsymbol{S}_i$. Since the energy resulting from the rearrangement of the magnetic moments is much lower than costs of the thermal excitations of itinerant electrons, we focus on fluctuations of the classical moments and assume that fermions are in their ground state [54]. Such fluctuations are expected to suppress ordering of the local moments, indirectly affecting the topological superconducting phase.

To estimate the critical temperature T_c up to which the topologically nontrivial state can persist, we have performed the MC simulations for the localized magnetic moments. Since the Hamiltonian (1) includes both the quantum (fermions) and the classical (localized magnetic moments) degrees of freedom, we apply the method used in Ref. [55]. At each MC step, a randomly chosen localized magnetic moment is rotated, the Hamiltonian (1) with an actual configuration of $\boldsymbol{S}_i$ is diagonalized, and the trial move is accepted or rejected according to the Metropolis criterion based on the free energy instead of the internal energy. During such a routine, we have computed the topological quantum number $\mathcal{Q}$ and various correlation functions. The great advantage of the MC method is that we do not need any particular ansatz for the magnetic order that is crucial for inspecting the self-organized structures composed of, e.g., several coexisting phases [42].

Most of our results refer to the magnetic moments confined to a plane, therefore, only the azimuthal angles ϕ_i have been varied in MC simulations. Section V presents some results for the case when this constraint is relaxed. In what follows, we discuss the most interesting results obtained within the aforementioned algorithm.

A. Correlation function

In Sec. III, we have inspected the long-range spiral ordering of the ground state. Here, we analyze how this order is affected by thermal fluctuations. In Fig. 5, we show the structure factor of the magnetic order $A(q) = 1/L \sum_{jk} e^{iq(j-k)} \langle \boldsymbol{S}_j \cdot \boldsymbol{S}_k \rangle$

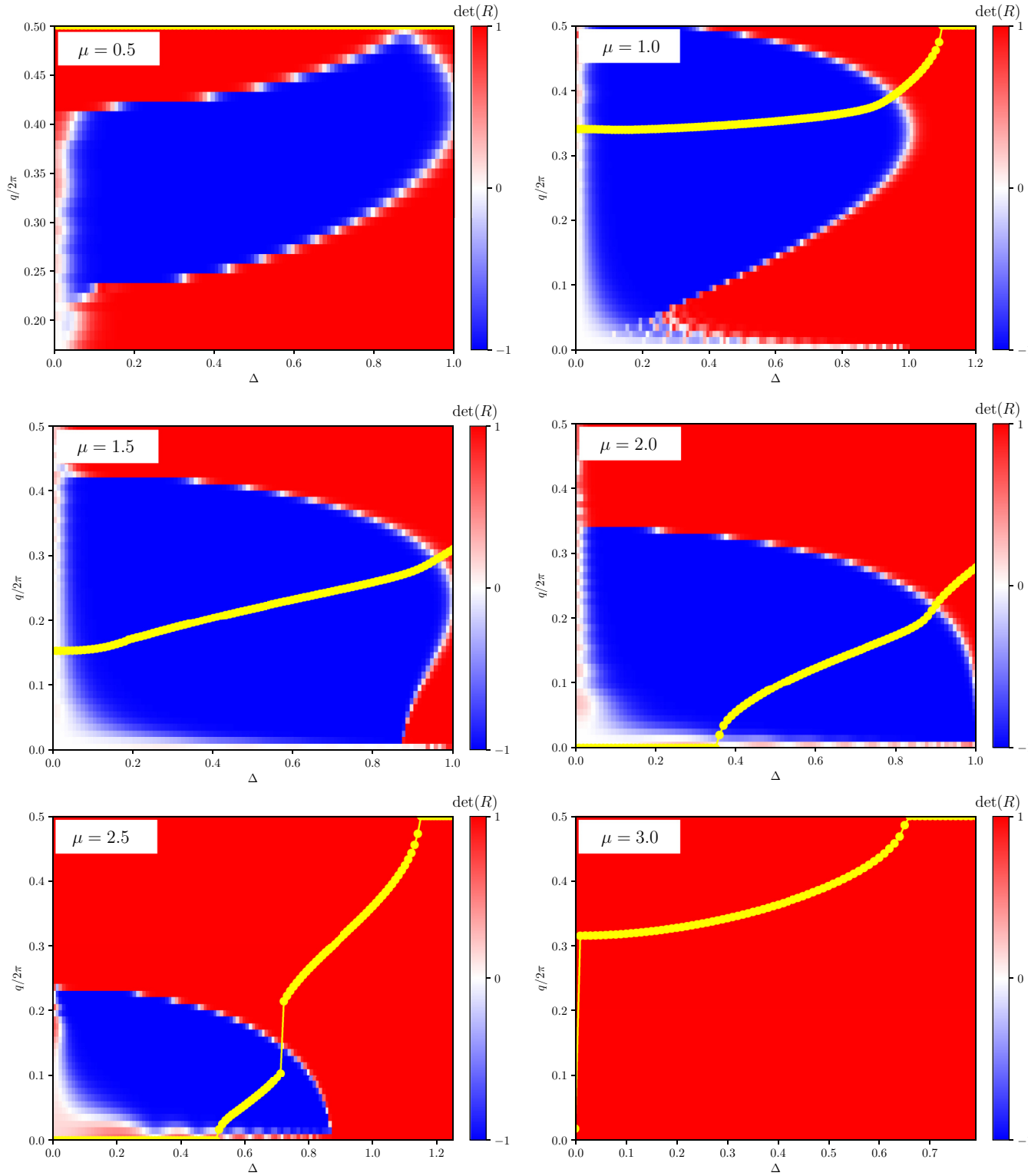

FIG. 3. Zero-temperature value of det(R) [see Eq. (7)] as a function of Δ and q obtained for 70 sites using $J = 2$ and different values of μ. The blue area [det(R) < 0] corresponds to topological, and the red one [det(R) > 0] corresponds to nontopological states, respectively. The yellow circles show q_*, minimizing the ground-state energy. Note that, for $\mu = 0.5$, q_* is equal to 0.5.

obtained at different temperatures as indicated. At very low temperatures, there is a narrow peak at $q = q_*$, indicating that magnetic configurations are nearly identical with the perfect zero-temperature long-range order. With increasing temperature, this peak remains at its original position, but its width substantially broadens, and its height is reduced. This signals that thermal fluctuations are detrimental for the magnetic ordering.

Stability of the spiral order against thermal fluctuations is determined by the strength and range of the effective

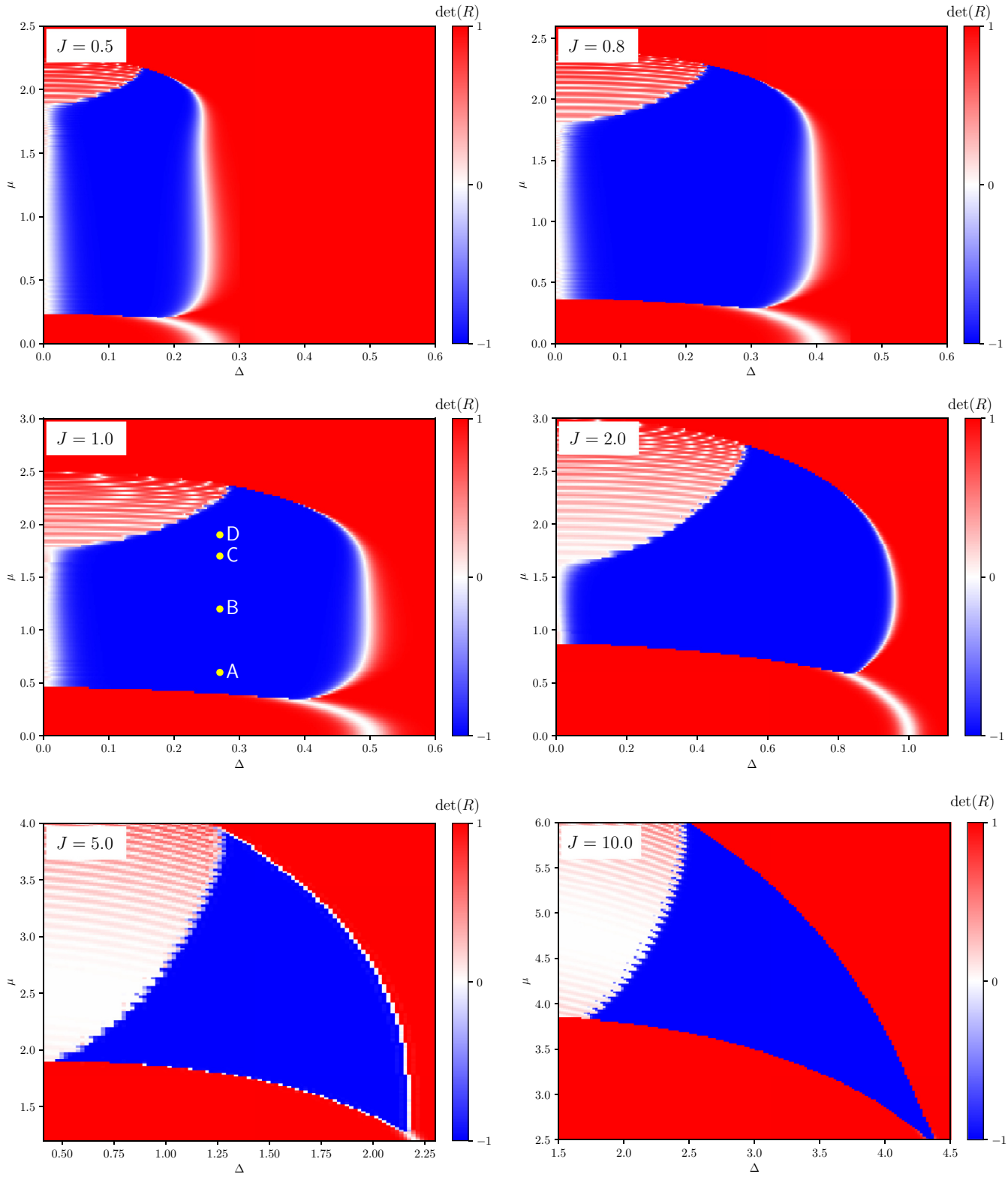

FIG. 4. Zero-temperature value of det(R) [see Eq. (7)] as a function of Δ and μ for different values of J, ranging from 0.5 to 10. The blue regions represent the topologically nontrivial phase [det$(R) < 0$] with the Majorana end modes. We have chosen q to minimize the ground-state energy for the chain of $L = 70$ lattice sites. The yellow circles labeled A–D indicate the parameters for which results are presented in Fig. 8.

interaction between the localized magnetic moments. The interaction is mediated by itinerant electrons which are paired through the proximity effect. Since the long-range type of the RKKY interaction in one-dimensional systems results from the gapless nature of excitations near the Fermi point, it is possible that, in our case, the effective interaction can differ from the standard one typical for metals. Proximity to a bulk superconductor can substantially affect its range,

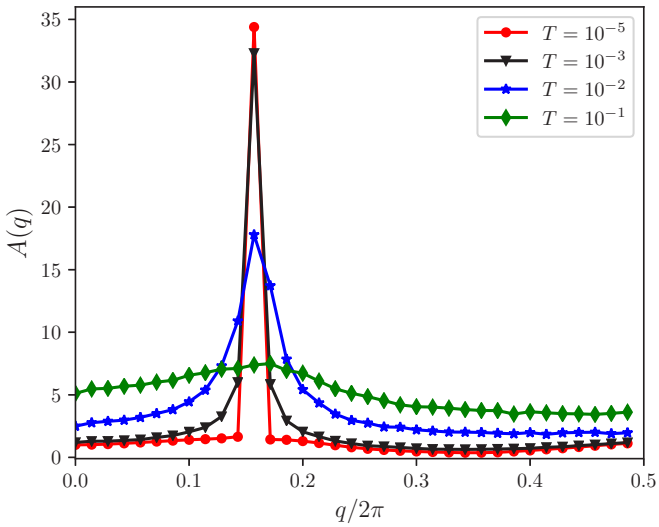

FIG. 5. The structure factor of the magnetic order obtained for $J = 1$ and the model parameters referring to point C in Fig. 4. Results are averaged over 10^5 statistically independent configurations generated during MC runs at temperatures $T = 10^{-5}$, 10^{-3}, 10^{-2}, and 10^{-1}.

which should be important for any magnetic order at finite temperatures [56]. In particular, if the interaction varies as $r^{-\alpha}$, the long-range order could exist for $\alpha < 2$ in the one-dimensional classical spin-S Heisenberg model [57,58].

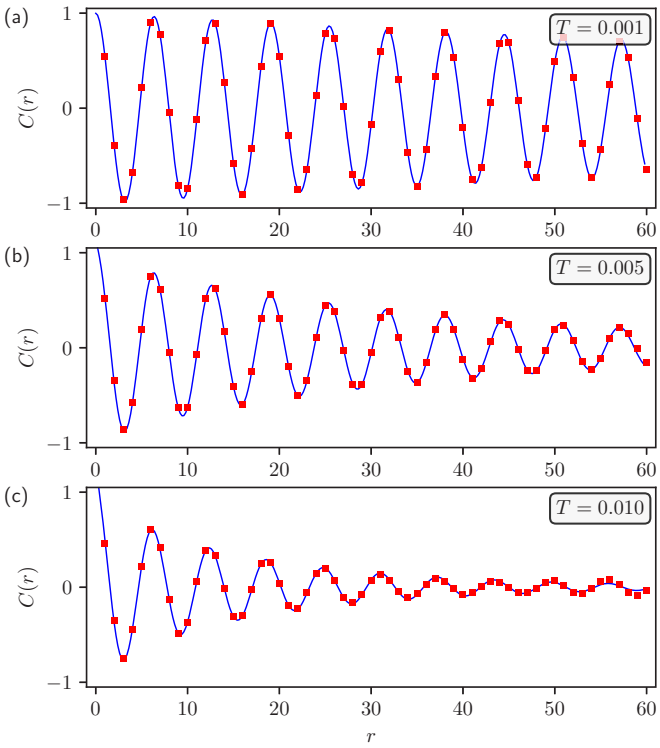

FIG. 6. Correlation function between the local magnetic moments (8) as a function of distance r obtained at representative temperatures for $\mu = 1.7$. The red thick points show the MC data, whereas the blue line is the best fit with a function defined in Eq. (9).

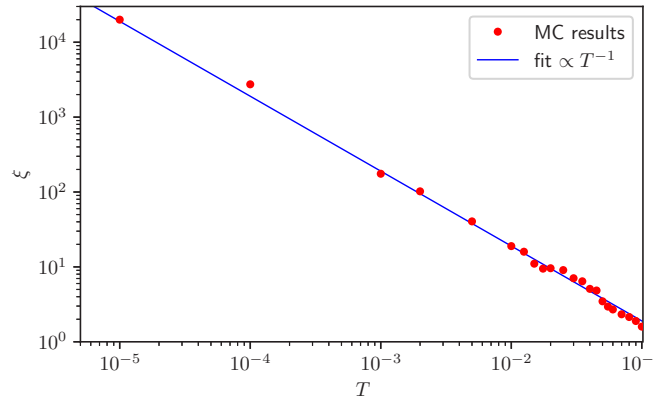

FIG. 7. Log-log plot of the correlation length versus temperature for the same model parameters as in Fig. 6. The red thick dots display the MC data, and the blue line is the best fit with a function $\xi(T) = AT^{-1}$.

To get insight into effective interactions between the localized moments and the role of the thermal effects, we have

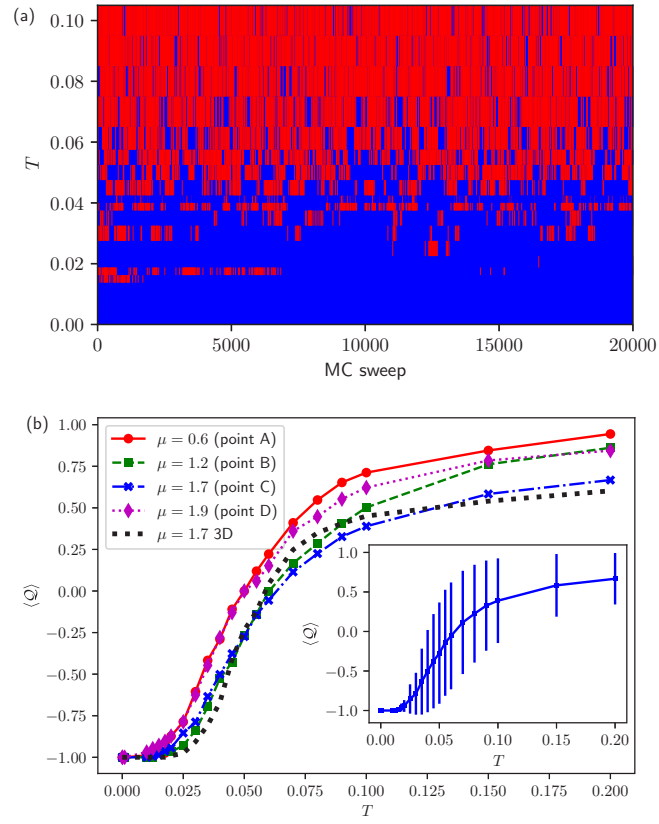

FIG. 8. (a) Variation of topological invariant $\mathcal{Q}$ during the MC sweeps obtained for varying temperature. The blue regions correspond to $\mathcal{Q} = -1$, and the red regions correspond to $\mathcal{Q} = +1$, respectively. The results refer to $J = 1$, $\mu = 1.7$, $\Delta = 0.27$ (point C in Fig. 4). (b) Temperature dependence of the invariant $\mathcal{Q}$ averaged over 10^5 MC sweeps for the model parameters indicated by points A–D in Fig. 4. The thick black dotted line marked as three dimensional "(3D)" shows $\mathcal{Q}$ calculated for point C under the assumption that the magnetic moments $\boldsymbol{S}_i$ are not confined to a plane (see Sec. V). The inset presents the standard deviation of $\mathcal{Q}$ obtained for point C.

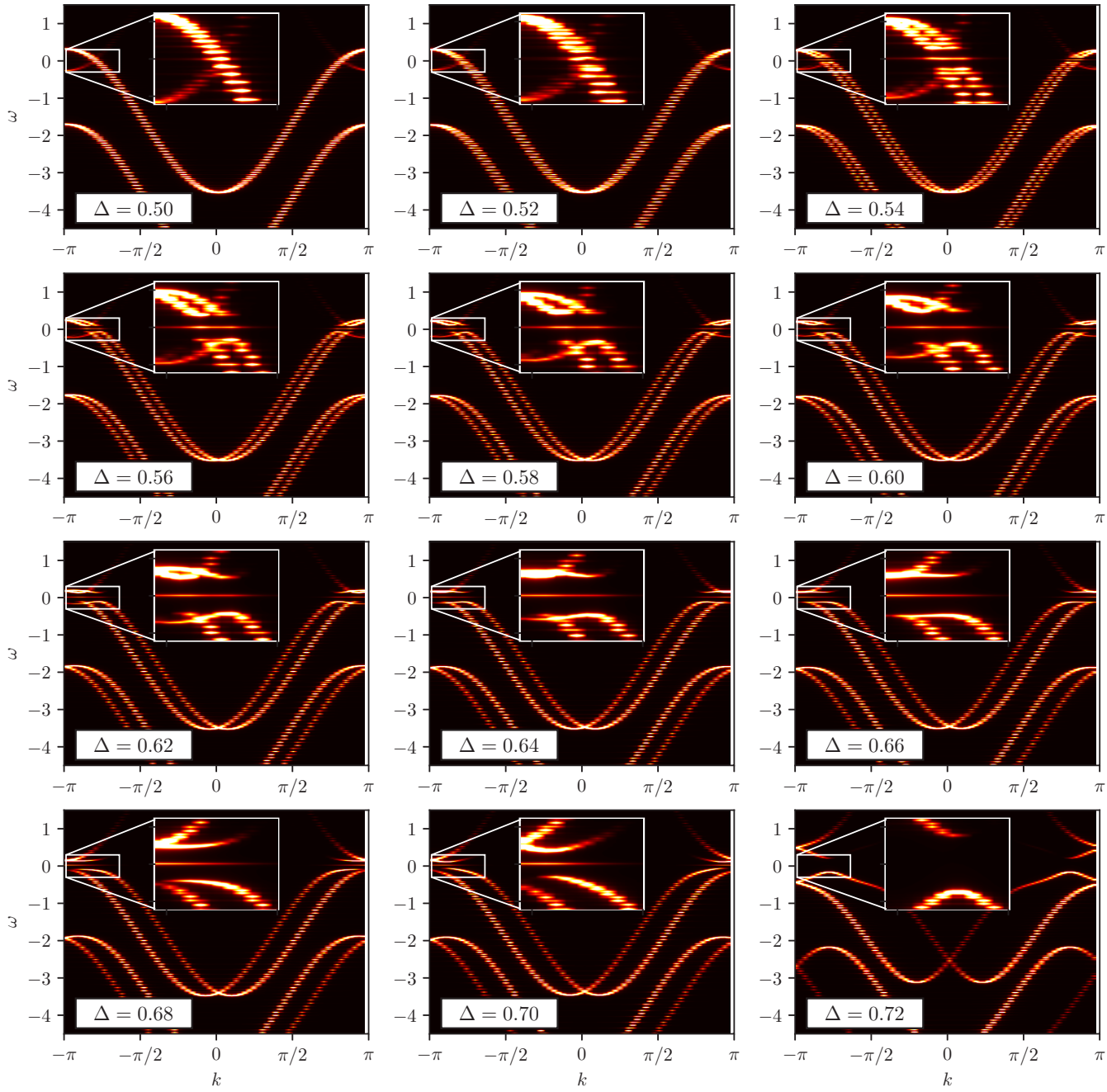

FIG. 9. Evolution of the zero-temperature spectral functions with respect to varying Δ obtained for $q = q_*$ which for the model parameter $\mu = 2.5$, $J = 2$ is shown by the yellow line in Fig. 3. The zoomed region displays the formation of the zero-energy mode. Note that the presence of this feature coincides with q_* being in the topological region (blue area in Fig. 3).

analyzed the correlation function defined as

$$C(r) = \frac{1}{L - r - 2s} \sum_{i=s}^{L-r-s} \langle \boldsymbol{S}_i \cdot \boldsymbol{S}_{i+r} \rangle, \tag{8}$$

where L denotes the nanochain length and s is a small offset introduced to minimize the finite-size effects. Results of our numerical MC computations obtained for three representative temperatures are presented by the thick red dots in Fig. 6. The simulations show that the exponential decay of the two-point correlation function has a power-law correction. The classical Ornstein-Zernike power $(d - 1)/2$, where d is the dimensionality of the system, vanishes in a one-dimensional system [59]. Here, however, the MC results can be very well fitted by

$$C(r) \propto \cos(qr)\, r^{-\alpha} e^{-r/\xi(T)}, \tag{9}$$

where α is small ($\alpha \ll 1$) and slightly temperature dependent. The major influence of thermal fluctuations is seen by the correlation length $\xi(T)$ (see Fig. 7). We have also treated q as a fitting parameter, but it turned out that, even at elevated temperatures, its value was very close to q_*, that minimizes the ground-state energy.

Fitting the MC results by $C(r)$ defined in Eq. (9) has enabled us to determine the temperature-dependent correlation length. As can be seen in Fig. 7, it diverges for $T \to 0$, indicating that the effective interaction is too short ranged to produce any long-range order at finite temperatures. Nevertheless, at sufficiently low temperatures, the correlation length is comparable to the nanowire length, therefore, the system remains in the topologically nontrivial state with the Majorana modes located at its edges. For unambiguous verification of such a possibility, we have directly calculated the topological properties of the system at finite temperatures (Sec. IV B).

B. Topological phase at finite temperatures

Figure 8(a) displays variation of the topological invariant $\mathcal{Q}$ during the MC runs performed at different temperatures (vertical axis). We have chosen the model parameters which guarantee the system to be in the topologically nontrivial phase at zero temperature (point C in Fig. 4, corresponding to $J = 1.0$). At this point, the system is in its topologically nontrivial state for chains of different lengths (see Fig. 19). We clearly note that with increasing temperature more and more frequently the system prefers the topologically trivial state. Such a gradual changeover from the topological to the nontopological phase depends on the chemical potential [Fig. 8(b)] and other parameters as well. Roughly speaking, for the chosen set of model parameters, the topological phase exists up to the critical temperature $T_c \sim 0.04$ (in units of the hopping integral). Considering typical values of $t \sim 10$ meV [34,35], this would yield the critical temperature for the topological superconducting phase $T_c \sim 5$ K, which is a more stringent limitation than all previous estimations [34,35,47].

C. Spectral functions

Another evidence for the detrimental influence of thermal effects on the topological superconductivity and the Majorana modes can be seen directly from the quasiparticle spectra of fermions. The spectral function,

$$A(k,\omega) = -\frac{1}{\pi}\mathrm{Im}\, G(k,\omega + i0^+) \tag{10}$$

can be obtained using the single-particle Green's function,

$$G(k,z)\delta(k-k') = \sum_{m,n}\langle \mathcal{G}_{mn}(z)\rangle e^{i(mk-nk')}. \tag{11}$$

Here, $\mathcal{G}_{mn}(z) = \{[z-H]^{-1}\}_{mn}$ is defined in the real space for a given configuration of the localized moments (recall that the lattice constant $a \equiv 1$), and $\langle\cdots\rangle$ denotes averaging over configurations generated in MC runs. For any particular (inhomogeneous) configuration of the localized moments, the Fourier transform of $\mathcal{G}_{mn}(z)$ depends on both k and k'. However, averaged over configurations, it becomes strongly peaked around $k = k'$. A finite width of this peak results from the finite size of the system and vanishes in the $L \to \infty$ limit.

Let us first inspect the spectral function (10) at zero temperature to demonstrate its characteristic features upon entering the topological regime. Figure 9 presents evolution of the low-energy spectrum, showing emergence of the zero-energy Majorana mode. For a given value of Δ we have computed the optimal pitch q_* of the ground state and then determined $A(k,\omega)$ for the model Hamiltonian (1) with such a particular configuration of the local moments S_i. In other words, at zero temperature, the averaging over configurations $\langle\cdots\rangle$ defined in Eq. (11) was not necessary. For the chosen value of $\mu = 2.5$, the pitch vector $q_*(\Delta)$ is shown by the yellow line in Fig. 3. In particular, we can note the qualitative change (from a topological to a nontopological phase) when Δ varies from 0.50 to 0.72, which corresponds to the abrupt jump of $q_*(\Delta)$ displayed in Fig. 3. The integrated spectral weight [total density of states (DOS)] for three characteristic points is presented in Fig. 10. Panel (a) shows DOS for $\Delta = 0.52$ where there is no gap in the energy spectrum. For $\Delta = 0.66$ [panel (b)], there is a gap with a well pronounced zero-energy Majorana mode. For $\Delta = 0.72$ [panel (c)], the gap still exists, but the system is not in the topological regime, so the Majorana mode is absent. Due to the correspondence between the present Hamiltonian and the one describing the Rashba chain, the spatial profile of the Majorana mode is very similar to what has been presented, e.g., in Fig. 6 of Ref. [60].

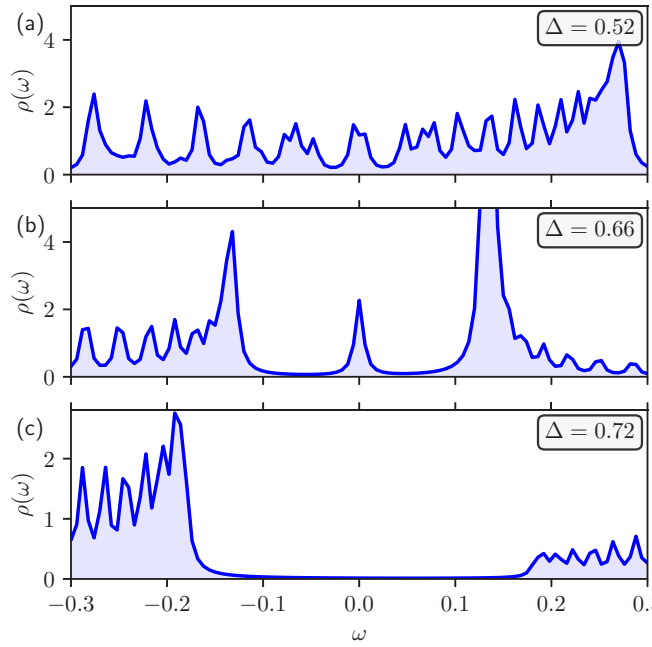

FIG. 10. The density of states for (a) $\Delta = 0.52$, (b) $\Delta = 0.66$, and (c) $\Delta = 72$. Other model parameters are the same as in Fig. 9. The irregular shape of the functions results from the finite length of the system ($L = 70$).

The influence of thermal effects of the spectral function (10) is illustrated for the representative set of model parameters in Fig. 11. At zero temperature, the Majorana mode (appearing near boundaries of the Brillouin zone as shown by the inset) is protected from the finite-energy Andreev quasiparticles by the topological gap. Upon increasing the temperature, such a topological gap gradually diminishes. This is accompanied by an ongoing disordering of the local magnetic moments leading to a broadening of all the spectral lines. Ultimately, at temperatures $T \simeq 0.05$, the topological gap is hardly visible, and the zero-energy feature merges with a continuum. Nonetheless, even at higher temperatures, we could still resolve some remnants of the overdamped zero-energy

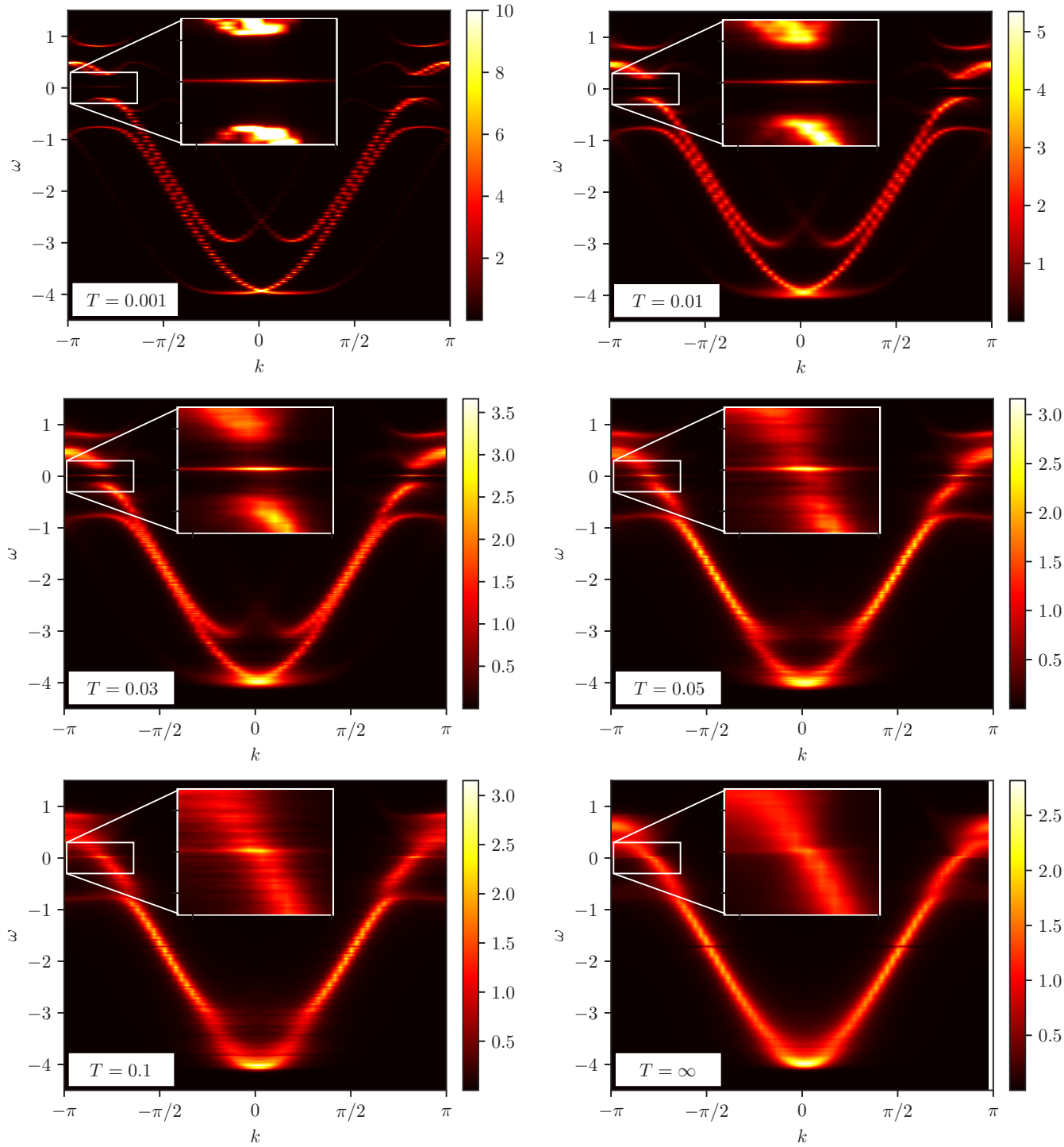

FIG. 11. The spectral function [defined in Eq. (10)] averaged over 10^3 statistically independent configurations of the localized moments $\{\boldsymbol{S}_i\}$. MC results are obtained for $J = 1$, $\mu = 1.7$, $\Delta = 0.27$, and several temperatures as indicated. The zoomed region displays the zero-energy mode.

mode. This brings us to the conclusion that the topological superconductivity vanishes near such a critical temperature in a continuous manner (such as a crossover rather than a typical phase transition). The temperature-induced suppression of the Majorana quasiparticles close to the system edges (not shown here) is very similar to detrimental influence caused by inhomogeneity of the Rashba chain (see Fig. 6 of Ref. [60]).

V. BEYOND COPLANAR ORDERING

Finally, we have checked whether deviation of the azimuthal angle of the local moments (3) from its coplanar value $\theta_i = \pi/2$ could affect the topological superconducting phase. For this purpose, we have performed MC simulations, treating both angles (θ_i, ϕ_i) on equal footing. To find the lowest-energy

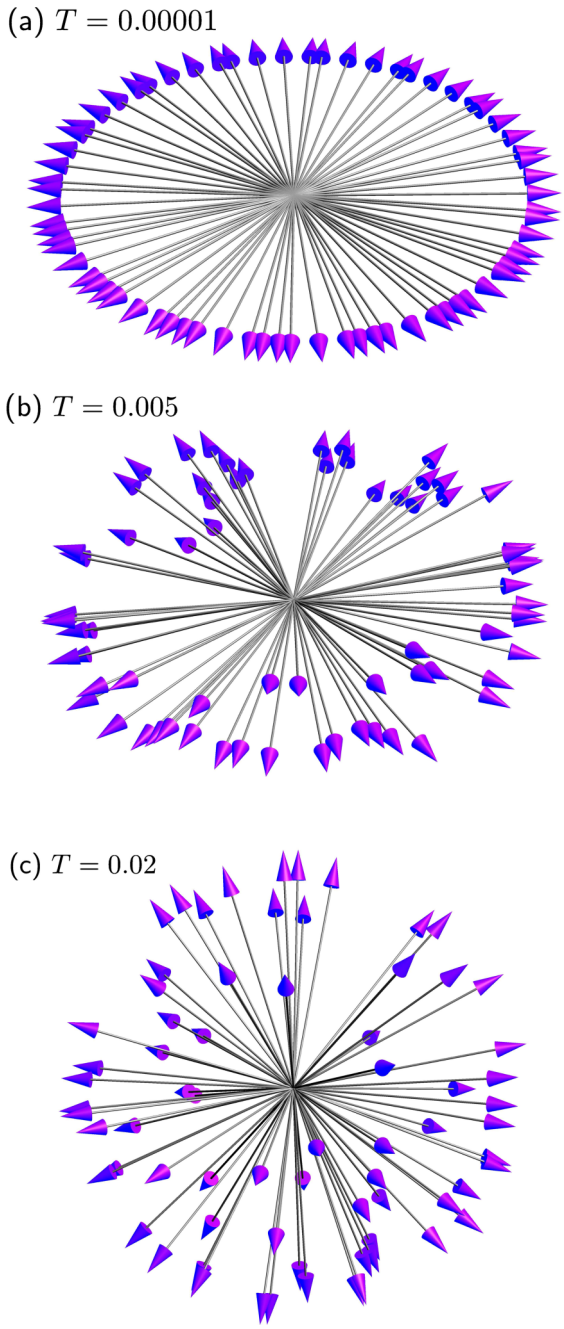

FIG. 12. Orientations of the localized magnetic moments at different temperatures. The model parameters correspond to point C in Fig. 4. For the sake of clearness, the origin of all these vectors has been collected to a common point and the average plane of the order tilted to be horizontal.

configuration of the localized magnetic moments, we used the simulated annealing method [61].

At very low temperatures, the local magnetic moments are arranged in a coplanar spiral, albeit now the plane of moments rotation is arbitrarily oriented, which reflects the symmetry of the Hamiltonian (1). This situation is illustrated in Fig. 12(a) where the moments have been shifted so that their origins are in the same point.

As a result, the zero-temperature phase diagrams are the same as in Fig. 4. With increasing temperature, the moments

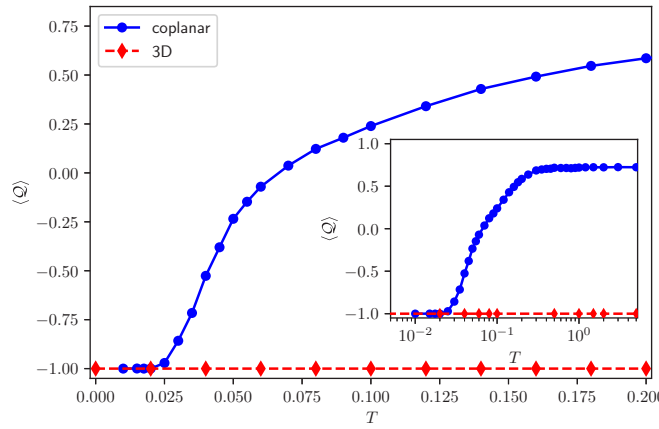

FIG. 13. Temperature dependence of the average topological invariant $\mathcal{Q}$ for coplanar configurations of the localized magnetic moments (blue solid line) and when their rotation is allowed in an arbitrary direction (red dashed line marked 3D). The inset shows the same but on a semilogarithmic scale for a wider range of temperatures. The model parameters are $J = 4$, $\Delta = 1.2$, and $\mu = 2$.

deviate from their coplanar arrangement (besides introducing in-plane disorder). Similar to the previously studied case where the moments were confined to a plane, it may lead to the destruction of the topological state. As the temperature increases, the topological region shrinks and usually eventually vanishes. An example of such a behavior is illustrated by the thick dotted black line in Fig. 8(b). One can note there that the temperature dependence of $\langle \mathcal{Q} \rangle$ is almost unaffected by the presence of the additional degree of freedom, which may suggest that fluctuations of the polar angle θ_i are rather irrelevant for stability of the topologically nontrivial superconducting phase.

This property, however, is not universal. Figure 13 shows the temperature dependence of $\langle \mathcal{Q} \rangle$ for a different set of the model parameters. In this case, the topological phase is destroyed by increasing temperature when only in-plane thermal fluctuations of the localized moments are allowed, but it survives to pretty high temperatures when they rotate freely in all three dimensions. Such intriguing behavior requires fine-tuning of the model parameters, and we have found only one region where the topological state is not destroyed at high temperatures. Figure 14 shows the average value of $\det(R)$ at zero and infinite temperatures. One can note that only for parameters close to the point marked by the white cross the averaged value of $\det(R)$ is equal to -1. This is the point for which the temperature dependence of $\langle \mathcal{Q} \rangle$ is presented in Fig. 13.

Extremely high temperatures in this case means that the local moments are completely randomly oriented. Of course, it does not imply that the topological state would survive up to arbitrarily high temperatures because, at some critical point, the superconducting state of the substrate would be destroyed. However, the magnitude of effective interactions between the localized moments is much smaller than the superconducting gap and other energies of the electronic subsystem. Therefore, in typical situations, i.e., when destruction of the helical order destroys also the topological state, this is the energy scale that usually determines the critical temperature.

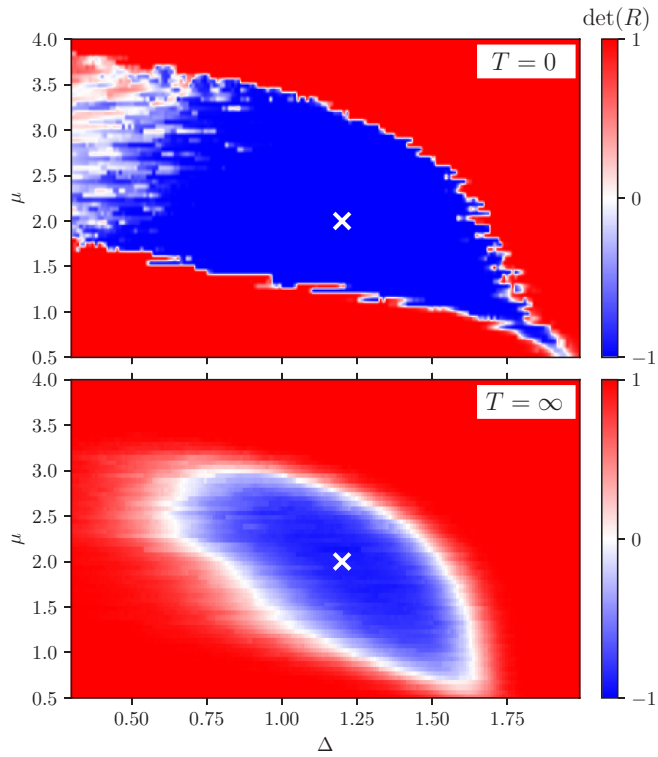

FIG. 14. The average value of det(R) at zero and infinite temperatures for $J = 4$. The white cross corresponds to parameters for which the temperature dependence of $\langle \mathcal{Q} \rangle$ is presented in Fig. 13.

Since, at high temperatures, there is no helical order, the model Hamiltonian (1) cannot be related to the scenario with the spin-orbit and Zeeman interactions [34,49]. However, it was shown in Ref. [28] that even without the helical order this Hamiltonian can have a topologically nontrivial state provided the localized magnetic moments point in different directions. To study how the ordering is destroyed by unrestricted thermal fluctuations, we parametrize the local moments in a way presented in Fig. 15. To distinguish the in-plane and out-of-plane types of fluctuations, we apply the following procedure. Using MC simulations, we generate large sets of statistically independent configurations of the local moments at different temperatures. The configurations are represented by unit vectors defined by $\hat{\boldsymbol{r}}_i = (\sin\theta_i \cos\phi_i, \sin\theta_i \sin\phi_i, \cos\theta_i)$, $i = 1, \ldots, L$. For each configuration, we use *singular value decomposition* to find plane $\mathcal{P}$ best fitted to the end points of these vectors. In Fig. 15, the horizontal gray circle represents this plane, and the blue arrows represent arbitrary two neighboring vectors $\hat{\boldsymbol{r}}_i$ and $\hat{\boldsymbol{r}}_{i+1}$. For each configuration, we calculate the angles α_i between vector $\hat{\boldsymbol{r}}_i$ and plane $\mathcal{P}$ and other angles γ_i between projections of $\hat{\boldsymbol{r}}_i$ and $\hat{\boldsymbol{r}}_{i+1}$ on plane $\mathcal{P}$. At low temperatures, the average values of these angles (for a single configuration) are $\overline{\alpha} \equiv 1/L \sum_i \alpha_i \approx 0$ and $\overline{\gamma} \equiv 1/L \sum_i \gamma_i \approx q_*$. We use the variance of α_i's and γ_i's around these values as a measure of the out-of-plane and in-plane fluctuations, respectively.

Figure 16 displays the fluctuations $\Delta\alpha \equiv \langle \overline{\alpha^2} - \overline{\alpha}^2 \rangle$ and $\Delta\gamma \equiv \langle \overline{\gamma^2} - \overline{\gamma}^2 \rangle$ with respect to temperature, where $\langle \cdots \rangle$ denotes averaging over configurations generated in MC runs.

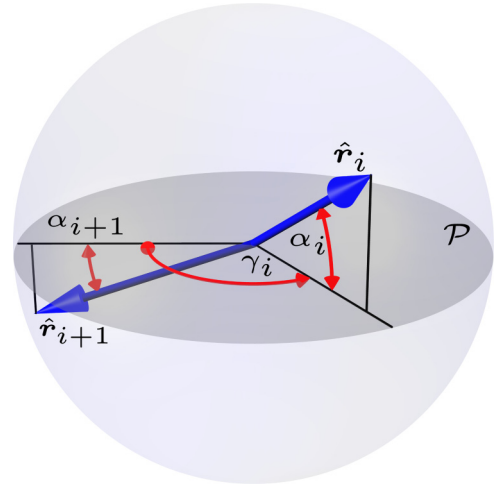

FIG. 15. Parametrization of directions of the local moments. The blue arrows marked $\hat{\boldsymbol{r}}_i$ and $\hat{\boldsymbol{r}}_{i+1}$ are unit vectors representing directions of two neighboring moments, the gray circle represents a plane $\mathcal{P}$ best fitted to the end points of all vectors $\hat{\boldsymbol{r}}_i$, $i = 1, \ldots, L$; α_i is an angle between vector $\hat{\boldsymbol{r}}_i$ and plane $\mathcal{P}$; γ_i is an angle between projections of vectors $\hat{\boldsymbol{r}}_i$ and $\hat{\boldsymbol{r}}_{i+1}$ on plane $\mathcal{P}$.

Both types of fluctuations vanish when $T \to 0$. It means that, in this limit, a perfect spiral order with a coplanar alignment is formed although the orientation of the plane is arbitrary. With increasing temperature, the in-plane fluctuations develop, and they dominate over the out-of-plane ones for $T < 10^{-3}$. At higher temperatures, both types of fluctuations significantly increase, and the alignment of the magnetic moments loses its coplanar character.

It is usually assumed that, for sufficiently large J, the electron spin is parallel to the localized magnetic moment. We

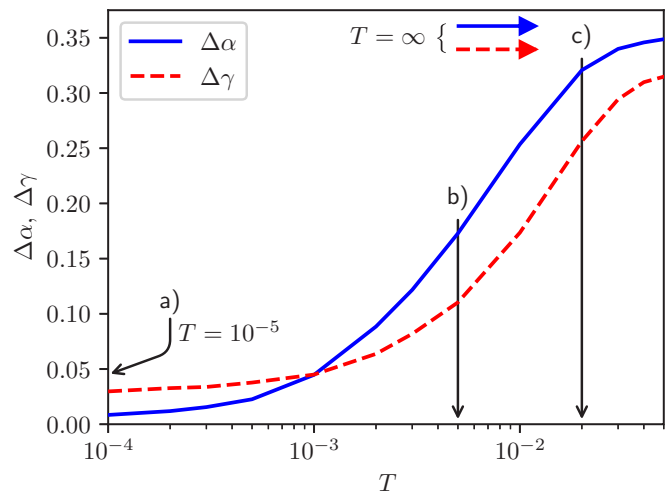

FIG. 16. Typical temperature dependence of the out-of-plane (blue solid line) and in-plane (red dashed line) fluctuations of the local moments. The horizontal arrows indicate the limiting values of $\Delta\alpha$ and $\Delta\gamma$ at $T = \infty$, i.e., for randomly oriented moments. The black arrows marked (a)–(c) indicate temperatures at which typical configurations are presented in Figs. 15(a)–15(c), respectively. The model parameters are the same as at point C in Fig. 4.

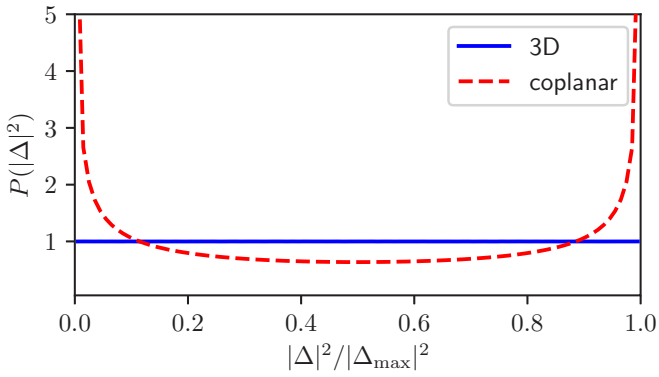

FIG. 17. Distributions of the squared magnitude of the pair potential $|\Delta_i|^2$ obtained for the nanowire with coplanar and three-dimensional magnetic moments as indicated.

have verified this assumption by calculating the correlation function $1/L\sum_i\langle \boldsymbol{S}_i\cdot\hat{\boldsymbol{s}}_i\rangle$. The results show that the electron spin is almost completely polarized along the localized magnetic moments for an *arbitrary* value of J. In such a case, the Hamiltonian (1) can be projected onto the lowest spin band and take a form of Kitaev's chain with additional hopping to the next-nearest neighbors [28]. In the effective Kitaev Hamiltonian, the pairing potential increases with increasing disorder of the magnetic moments and can drive the system into the topological phase. This can explain that, although the spiral ordering is destroyed at high temperatures, another mechanism can still preserve the system in its nontrivial state as marked by the red line in Fig. 13.

One may ask why the same mapping onto the Kitaev model does not lead to a high-temperature topological state in the case when the local moments are confined to a plane? It has been shown in Ref. [28] that the pair potential Δ_i in the effective model is proportional to

$$\Delta_i \propto -\sin\frac{\theta_i}{2}\cos\frac{\theta_{i+1}}{2}e^{i\phi_i}+\cos\frac{\theta_i}{2}\sin\frac{\theta_{i+1}}{2}e^{i\phi_{i+1}}, \tag{12}$$

that for $\theta_i=\pi/2$ (the coplanar arrangement) reduces to

$$\Delta_i \propto \tfrac{1}{2}(e^{i\phi_{i+1}}-e^{i\phi_i}). \tag{13}$$

In the 3D case at infinite temperatures, the directions of vectors $\hat{\boldsymbol{r}}_i$ are uniformly distributed in a full 4π solid angle.

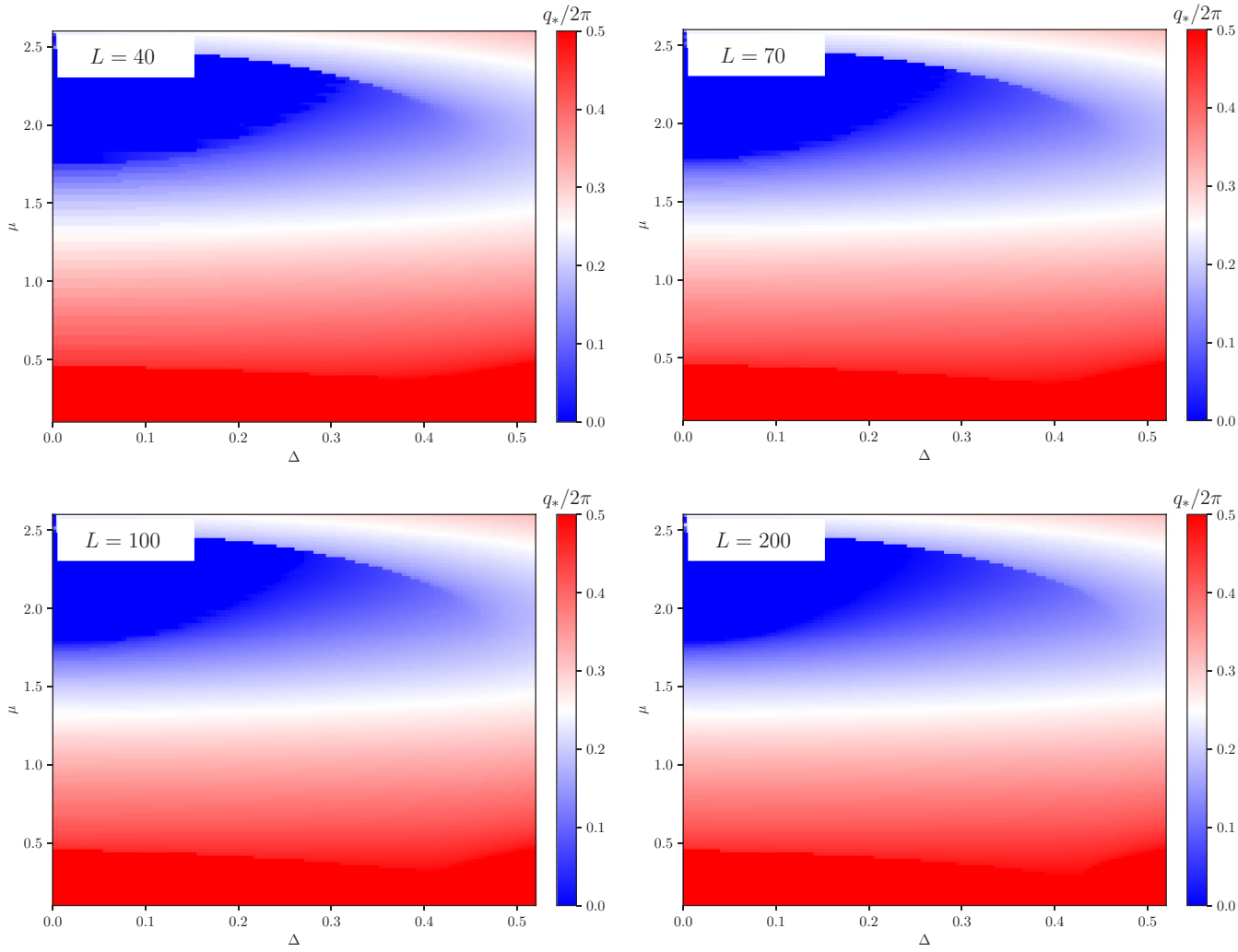

FIG. 18. The pitch vector q_* obtained at zero temperature for $J=1$ and several sizes, ranging from $L=40$ to $L=200$. The model parameters are the same as in Fig. 4.

For the coplanar confining, only ϕ_i's are uniformly distributed from 0 to 2π, whereas $\theta_i = \pi/2$. The corresponding distributions of the squared pair potential $|\Delta_i|^2$ are shown in Fig. 17. One can note that, in the 3D case, it is random with a box distribution between 0 and $|\Delta|^2_{\max}$, whereas, for coplanar confining, it is strongly peaked around 0 and $|\Delta|^2_{\max}$, resembling almost a binary distribution. We believe the latter distribution may be much more destructive for the topological state by leading to the formation of Griffiths-like phases in a disordered chain [60,62,63].

VI. SUMMARY

We have investigated the stability of the topologically nontrivial superconducting phase of itinerant electrons coupled to the local magnetic moments in the finite-length nanowire proximitized to a *s*-wave superconductor. We have performed the MC simulations, considering various configurations of such local moments constrained on a plane and oriented arbitrarily in all three directions. We have focused on the role played by thermal fluctuations. MC simulations clearly indicate that self-organization of the local moments into the spiral order gradually ceases upon increasing the temperature. We have found the universal scaling of the correlation function for the localized magnetic moments (8) and determined the coherence length, revealing its characteristic temperature dependence $\xi(T) \propto 1/T$.

Our MC data for the topological invariant and analysis of the quasiparticle spectrum both unambiguously show the upper (critical) temperature T_c, above which the topological nature of the superconducting phase no longer exists. When approaching this critical temperature from below, there occurs a gradual reduction of the topological gap, protecting the zero-energy mode from the finite-energy (Andreev-type) quasiparticles so that, at $T \to T_c$, the Majorana modes get overdamped. Our quantitative estimations show that $T_c \sim 0.05$ (in units of the hopping integral) that in realistic systems would yield $T_c \sim 6$ K. Such an upper limit for the existence of the topological superconducting phase could be important for experimental and theoretical studies of the Majorana quasiparticles in the condensed-matter and the ultracold atom systems. This evaluation should also be taken into account when considering future applications of the Majorana quasiparticles for quantum computing.

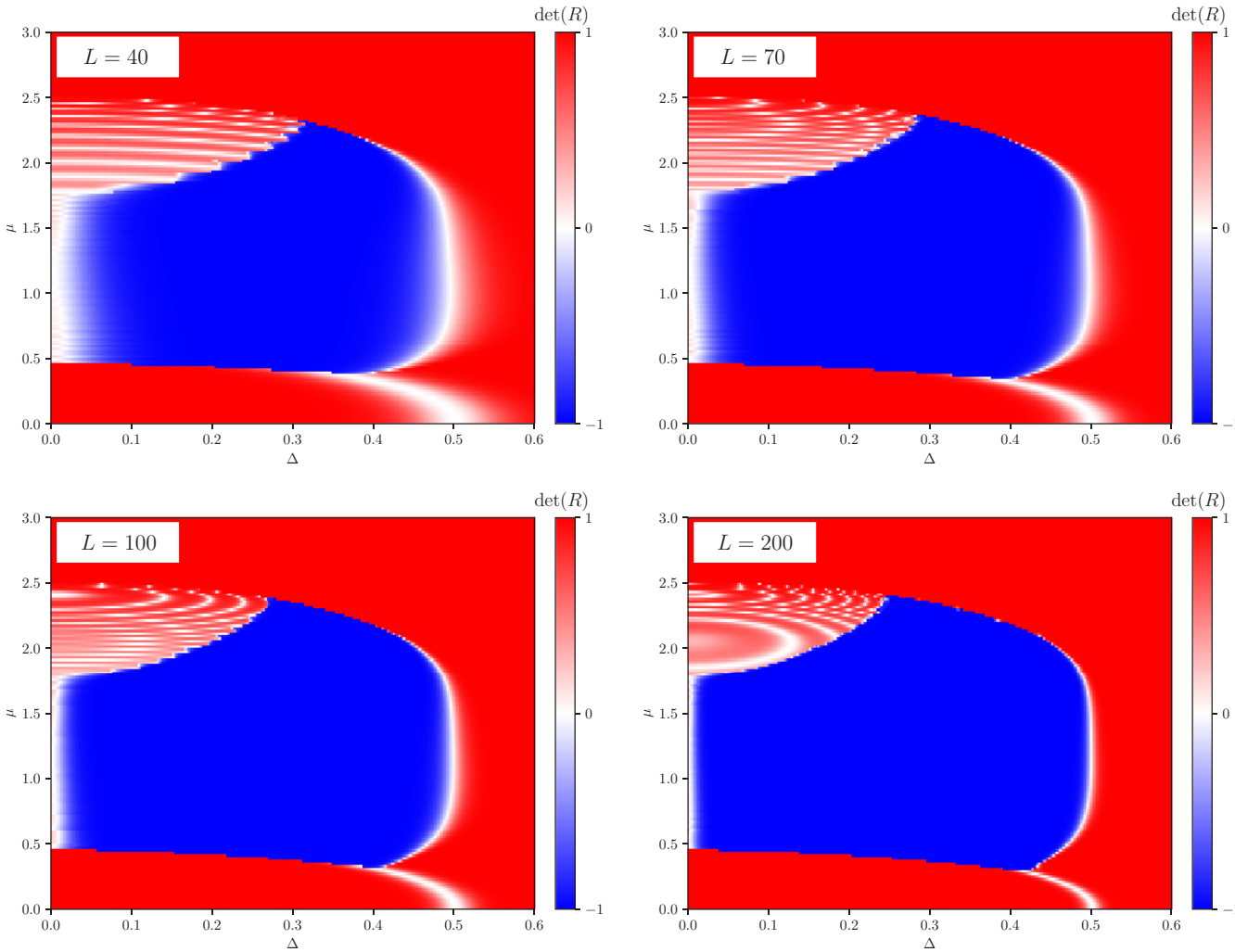

FIG. 19. det(R) obtained for $J = 1$ and several sizes, ranging from $L = 40$ to $L = 200$. Computations have been performed for the same model parameters as in Fig. 4.

The approach we used in this paper is quite general, and thus, the model can be easily extended by taking into account other mechanisms which affect stability of the topological phase, such as the spin-orbit coupling, direct interaction between the localized moments, different kinds of disorder, or an external magnetic field.

ACKNOWLEDGMENTS

We acknowledge discussions with J. Klinovaja and J. Paaske. This work was supported by the National Science Centre (Poland) under Contracts No. DEC-2018/29/B/ST3/01892 (A.G.-G. and M.M.M.) and No. DEC-2017/27/B/ST3/01911 (T.D.).

APPENDIX: FINITE-SIZE SCALING

In the scenario based on the Rashba nanowire proximitized to a bulk superconductor, a sharp transition from the topologically trivial to the nontrivial regime has been predicted only for infinitely long wires, and it has been emphasized [64] that finite-size effects would smooth it into a crossover. Due to correspondence between systems with the spin-orbit and Zeeman interactions and systems with the spiral ordering of localized moments, the same effect can be expected for the present model described by the Hamiltonian (1). To verify it, we performed additional calculations for various lengths L of nanowires, comprising 40 to 200 sites.

Pitch vector q_* of the ground state (Fig. 18) and diagrams of the topological superconducting phase (Fig. 19) clearly indicate that: (i) q_* is hardly affected by nanowire length L, (ii) total area of the topological phase in the parameter space slightly increases with increasing L, and (iii) boundaries of the topological region are sharper for longer nanowires. In both these figures, one can note that the size dependence is weak, and, already, for $L = 40$, the main properties of the system are clearly visible.

Observations (i) and (ii) suggest that a tendency towards formation of the topological state (*topofilia*) should be valid for sufficiently long nanochains. With regard to observation (iii), it indicates that, in the studied system, the finite-size effects smooth out the topological transition. This is visible in Fig. 19 for $L = 40$ where the white area shows such a transition between the topologically trivial and the nontrivial regions. Finite-size effects are also important for splitting of the Majorana end modes when their overlap is sizable (for short nanowires).

[1] A. Santos, M. J. Deen, and L. F. Marsal, Low-cost fabrication technologies for nanostructures: State-of-the-art and potential, Nanotechnology **26**, 042001 (2015).

[2] C. Zhang, H.-Z. Lu, S.-Q. Shen, Y. P. Chen, and F. Xiu, Towards the manipulation of topological states of matter: A perspective from electron transport, Sci. Bull. **63**, 580 (2018).

[3] A. Y. Kitaev, Unpaired Majorana fermions in quantum wires, Phys.-Usp. **44**, 131 (2001).

[4] M. T. Deng, C. L. Yu, G. Y. Huang, M. Larsson, P. Caroff, and H. Q. Xu, Anomalous zero-bias conductance peak in a Nb–InSb nanowire–Nb hybrid device, Nano Lett. **12**, 6414 (2012).

[5] V. Mourik, K. Zuo, S. M. Frolov, S. R. Plissard, E. P. A. M. Bakkers, and L. P. Kouwenhoven, Signatures of Majorana fermions in hybrid superconductor-semiconductor nanowire devices, Science **336**, 1003 (2012).

[6] A. Das, Y. Ronen, Y. Most, Y. Oreg, M. Heiblum, and H. Shtrikman, Zero-bias peaks and splitting in an Al–InAs nanowire topological superconductor as a signature of Majorana fermions, Nat. Phys. **8**, 887 (2012).

[7] A. D. K. Finck, D. J. Van Harlingen, P. K. Mohseni, K. Jung, and X. Li, Anomalous Modulation of a Zero-Bias Peak in a Hybrid Nanowire-Superconductor Device, Phys. Rev. Lett. **110**, 126406 (2013).

[8] M. T. Deng, S. Vaitiekenas, E. B. Hansen, J. Danon, M. Leijnse, K. Flensberg, J. Nygård, P. Krogstrup, and C. M. Marcus, Majorana bound state in a coupled quantum-dot hybrid-nanowire system, Science **354**, 1557 (2016).

[9] F. Nichele, A. C. C. Drachmann, A. M. Whiticar, E. C. T. O'Farrell, H. J. Suominen, A. Fornieri, T. Wang, G. C. Gardner, C. Thomas, A. T. Hatke, P. Krogstrup, M. J. Manfra, K. Flensberg, and C. M. Marcus, Scaling of Majorana Zero-Bias Conductance Peaks, Phys. Rev. Lett. **119**, 136803 (2017).

[10] R. M. Lutchyn, E. P. A. M. Bakkers, L. P. Kouwenhoven, P. Krogstrup, C. M. Marcus, and Y. Oreg, Majorana zero modes in superconductor-semiconductor heterostructures, Nat. Rev. Mater. **3**, 52 (2018).

[11] Ö. Gül, H. Zhang, J. D. S. Bommer, M. W. A. de Moor, D. Car, S. R. Plissard, E. P. A. M. Bakkers, A. Geresdi, K. Watanabe, T. Taniguchi, and L. P. Kouwenhoven, Ballistic Majorana nanowire devices, Nat. Nanotechnol. **13**, 192 (2018).

[12] S. Nadj-Perge, I. K. Drozdov, J. Li, H. Chen, S. Jeon, J. Seo, A. H. MacDonald, B. A. Bernevig, and A. Yazdani, Observation of Majorana fermions in ferromagnetic atomic chains on a superconductor, Science **346**, 602 (2014).

[13] R. Pawlak, M. Kisiel, J. Klinovaja, T. Meier, S. Kawai, T. Glatzel, D. Loss, and E. Meyer, Probing atomic structure and Majorana wavefunctions in mono-atomic Fe chains on superconducting Pb surface, npj Quantum Information **2**, 16035 (2016).

[14] B. E. Feldman, M. T. Randeria, J. Li, S. Jeon, Y. Xie, Z. Wang, I. K. Drozdov, B. A. Bernevig, and A. Yazdani, High-resolution studies of the Majorana atomic chain platform, Nat. Phys. **13**, 286 (2016).

[15] M. Ruby, B. W. Heinrich, Y. Peng, F. von Oppen, and K. J. Franke, Exploring a proximity-coupled Co chain on Pb (110) as a possible Majorana platform, Nano Lett. **17**, 4473 (2017).

[16] S. Jeon, Y. Xie, J. Li, Z. Wang, B. A. Bernevig, and A. Yazdani, Distinguishing a Majorana zero mode using spin-resolved measurements, Science **358**, 772 (2017).

[17] H. Kim, A. Palacio-Morales, T. Posske, L. Rózsa, K. Palotás, L. Szunyogh, M. Thorwart, and R. Wiesendanger, Toward tailoring Majorana bound states in artificially constructed magnetic atom chains on elemental superconductors, Sci. Adv. **4**, eaar5251 (2018).

[18] C. Nayak, S. H. Simon, A. Stern, M. Freedman, and S. Das Sarma, Non-Abelian anyons and topological quantum computation, Rev. Mod. Phys. **80**, 1083 (2008).

[19] D. Aasen, M. Hell, R. V. Mishmash, A. Higginbotham, J. Danon, M. Leijnse, T. S. Jespersen, J. A. Folk, C. M. Marcus, K. Flensberg, and J. Alicea, Milestones toward Majorana-based quantum computing, Phys. Rev. X **6**, 031016 (2016).

[20] T. Karzig, C. Knapp, R. M. Lutchyn, P. Bonderson, M. B. Hastings, C. Nayak, J. Alicea, K. Flensberg, S. Plugge, Y. Oreg, C. M. Marcus, and M. H. Freedman, Scalable designs for quasiparticle-poisoning-protected topological quantum computation with Majorana zero modes, Phys. Rev. B **95**, 235305 (2017).

[21] X. Liu, X. Li, D.-L. Deng, X.-J. Liu, and S. Das Sarma, Majorana spintronics, Phys. Rev. B **94**, 014511 (2016).

[22] M. Sato and S. Fujimoto, Topological phases of noncentrosymmetric superconductors: Edge states, Majorana fermions, and non-Abelian statistics, Phys. Rev. B **79**, 094504 (2009).

[23] M. Sato, Y. Takahashi, and S. Fujimoto, Non-Abelian Topological Order in *s*-Wave Superfluids of Ultracold Fermionic Atoms, Phys. Rev. Lett. **103**, 020401 (2009).

[24] M. Sato, Y. Takahashi, and S. Fujimoto, Non-Abelian topological orders and Majorana fermions in spin-singlet superconductors, Phys. Rev. B **82**, 134521 (2010).

[25] J. Klinovaja and D. Loss, Composite Majorana fermion wave functions in nanowires, Phys. Rev. B **86**, 085408 (2012).

[26] D. Chevallier, D. Sticlet, P. Simon, and C. Bena, Mutation of Andreev into Majorana bound states in long superconductor-normal and superconductor-normal-superconductor junctions, Phys. Rev. B **85**, 235307 (2012).

[27] D. Chevallier, P. Simon, and C. Bena, From Andreev bound states to Majorana fermions in topological wires on superconducting substrates: A story of mutation, Phys. Rev. B **88**, 165401 (2013).

[28] T.-P. Choy, J. M. Edge, A. R. Akhmerov, and C. W. J. Beenakker, Majorana fermions emerging from magnetic nanoparticles on a superconductor without spin-orbit coupling, Phys. Rev. B **84**, 195442 (2011).

[29] I. Martin and A. F. Morpurgo, Majorana fermions in superconducting helical magnets, Phys. Rev. B **85**, 144505 (2012).

[30] M. Kjaergaard, K. Wölms, and K. Flensberg, Majorana fermions in superconducting nanowires without spin-orbit coupling, Phys. Rev. B **85**, 020503(R) (2012).

[31] S. Nadj-Perge, I. K. Drozdov, B. A. Bernevig, and A. Yazdani, Proposal for realizing Majorana fermions in chains of magnetic atoms on a superconductor, Phys. Rev. B **88**, 020407(R) (2013).

[32] B. Braunecker and P. Simon, Interplay Between Classical Magnetic Moments and Superconductivity in Quantum One-Dimensional Conductors: Toward a Self-Sustained Topological Majorana Phase, Phys. Rev. Lett. **111**, 147202 (2013).

[33] F. Pientka, L. I. Glazman, and F. von Oppen, Topological superconducting phase in helical Shiba chains, Phys. Rev. B **88**, 155420 (2013).

[34] J. Klinovaja, P. Stano, A. Yazdani, and D. Loss, Topological Superconductivity and Majorana Fermions in RKKY Systems, Phys. Rev. Lett. **111**, 186805 (2013).

[35] M. M. Vazifeh and M. Franz, Self-Organized Topological State with Majorana Fermions, Phys. Rev. Lett. **111**, 206802 (2013).

[36] I. Reis, D. J. J. Marchand, and M. Franz, Self-organized topological state in a magnetic chain on the surface of a superconductor, Phys. Rev. B **90**, 085124 (2014).

[37] J. Li, H. Chen, I. K. Drozdov, A. Yazdani, B. A. Bernevig, and A. H. MacDonald, Topological superconductivity induced by ferromagnetic metal chains, Phys. Rev. B **90**, 235433 (2014).

[38] F. Pientka, L. I. Glazman, and F. von Oppen, Unconventional topological phase transitions in helical Shiba chains, Phys. Rev. B **89**, 180505(R) (2014).

[39] Y. Kim, M. Cheng, B. Bauer, R. M. Lutchyn, and S. Das Sarma, Helical order in one-dimensional magnetic atom chains and possible emergence of Majorana bound states, Phys. Rev. B **90**, 060401(R) (2014).

[40] A. Heimes, P. Kotetes, and G. Schön, Majorana fermions from Shiba states in an antiferromagnetic chain on top of a superconductor, Phys. Rev. B **90**, 060507(R) (2014).

[41] Y. Peng, F. Pientka, L. I. Glazman, and F. von Oppen, Strong Localization of Majorana End States in Chains of Magnetic Adatoms, Phys. Rev. Lett. **114**, 106801 (2015).

[42] W. Hu, R. T. Scalettar, and R. R. P. Singh, Interplay of magnetic order, pairing, and phase separation in a one-dimensional spin-fermion model, Phys. Rev. B **92**, 115133 (2015).

[43] P. M. R. Brydon, S. Das Sarma, H.-Y. Hui, and J. D. Sau, Topological Yu-Shiba-Rusinov chain from spin-orbit coupling, Phys. Rev. B **91**, 064505 (2015).

[44] M. Schecter, M. S. Rudner, and K. Flensberg, Spin-Lattice Order in One-Dimensional Conductors: Beyond the RKKY Effect, Phys. Rev. Lett. **114**, 247205 (2015).

[45] A. Heimes, D. Mendler, and P. Kotetes, Interplay of topological phases in magnetic adatom-chains on top of a Rashba superconducting surface, New J. Phys. **17**, 023051 (2015).

[46] W. Hu, R. T. Scalettar, and R. R. P. Singh, Erratum: Interplay of magnetic order, pairing, and phase separation in a one-dimensional spin-fermion model [Phys. Rev. B **92**, 115133 (2015)], Phys. Rev. B **93**, 119903(E) (2016).

[47] B. Braunecker and P. Simon, Self-stabilizing temperature-driven crossover between topological and nontopological ordered phases in one-dimensional conductors, Phys. Rev. B **92**, 241410(R) (2015).

[48] M. Schecter, K. Flensberg, M. H. Christensen, B. M. Andersen, and J. Paaske, Self-organized topological superconductivity in a Yu-Shiba-Rusinov chain, Phys. Rev. B **93**, 140503(R) (2016).

[49] B. Braunecker, G. I. Japaridze, J. Klinovaja, and D. Loss, Spin-selective Peierls transition in interacting one-dimensional conductors with spin-orbit interaction, Phys. Rev. B **82**, 045127 (2010).

[50] Formally, we work in the large-spin regime $S \to \infty$ with a finite value of $JS = \text{const}$. For the sake of simplicity, we assume $S = 1$ and use J to measure the coupling between the localized moments and the electron spin.

[51] A. R. Akhmerov, J. P. Dahlhaus, F. Hassler, M. Wimmer, and C. W. J. Beenakker, Quantized Conductance at the Majorana Phase Transition in a Disordered Superconducting Wire, Phys. Rev. Lett. **106**, 057001 (2011).

[52] I. C. Fulga, F. Hassler, A. R. Akhmerov, and C. W. J. Beenakker, Scattering formula for the topological quantum number of a disordered multimode wire, Phys. Rev. B **83**, 155429 (2011).

[53] M. H. Christensen, M. Schecter, K. Flensberg, B. M. Andersen, and J. Paaske, Spiral magnetic order and topological

superconductivity in a chain of magnetic adatoms on a two-dimensional superconductor, Phys. Rev. B **94**, 144509 (2016).

[54] J. Schliemann, J. König, and A. H. MacDonald, Monte Carlo study of ferromagnetism in (III,Mn)V semiconductors, Phys. Rev. B **64**, 165201 (2001).

[55] M. M. Maśka and K. Czajka, Thermodynamics of the two-dimensional falicov-kimball model: A classical Monte Carlo study, Phys. Rev. B **74**, 035109 (2006).

[56] N. D. Mermin and H. Wagner, Absence of Ferromagnetism or Antiferromagnetism in One- or Two-Dimensional Isotropic Heisenberg Models, Phys. Rev. Lett. **17**, 1133 (1966).

[57] J. B. Rogers and C. J. Thompson, Absence of long-range order in one-dimensional spin systems, J. Stat. Phys. **25**, 669 (1981).

[58] J. Fröhlich, R. Israel, E. H. Lieb, and B. Simon, Phase transitions and reflection positivity. i. general theory and long range lattice models, Commun. Math. Phys. **62**, 1 (1978).

[59] J. Cardy, *Scaling and Renormalization in Statistical Physics*, Cambridge Lecture Notes in Physics (Cambridge University Press, Cambridge, UK, 1996).

[60] M. M. Maśka, A. Gorczyca-Goraj, J. Tworzydło, and T. Domański, Majorana quasiparticles of an inhomogeneous Rashba chain, Phys. Rev. B **95**, 045429 (2017).

[61] S. Kirkpatrick, C. D. Gelatt, and M. P. Vecchi, Optimization by simulated annealing, Science **220**, 671 (1983).

[62] S. S. Hegde and S. Vishveshwara, Majorana wave-function oscillations, fermion parity switches, and disorder in Kitaev chains, Phys. Rev. B **94**, 115166 (2016).

[63] J. Wang and S. Chakravarty, Binary disorder in quantum Ising chains and induced Majorana zero modes, arXiv:1808.04481.

[64] R. V. Mishmash, D. Aasen, A. P. Higginbotham, and J. Alicea, Approaching a topological phase transition in Majorana nanowires, Phys. Rev. B **93**, 245404 (2016).